Relaxation of strongly coupled binary ionic mixtures in the coupled mode regime

Cite as: Phys. Plasmas **28**, 062302 (2021); https://doi.org/10.1063/5.0048030
Submitted: 18 February 2021 . Accepted: 04 May 2021 . Published Online: 03 June 2021

Luciano G. Silvestri, R. Tucker Sprenkle, Scott D. Bergeson, and Michael M. Murillo

Physics of Plasmas ARTICLE scitation.org/journal/php

Relaxation of strongly coupled binary ionic mixtures in the coupled mode regime

Cite as: Phys. Plasmas **28**, 062302 (2021); doi: 10.1063/5.0048030
Submitted: 18 February 2021 · Accepted: 4 May 2021 ·
Published Online: 3 June 2021

Luciano G. Silvestri,[1,a)] R. Tucker Sprenkle,[2] Scott D. Bergeson,[2] and Michael M. Murillo[1]

AFFILIATIONS

[1]Department of Computational Mathematics, Science and Engineering, Michigan State University, East Lansing, Michigan 48824, USA
[2]Department of Physics and Astronomy, Brigham Young University, Provo, Utah 84602, USA

Note: This paper is part of the Special Collection: Transport in Non-Ideal, Multi-Species Plasmas.
[a)]**Author to whom correspondence should be addressed:** silves28@msu.edu

ABSTRACT

Understanding ion transport in plasma mixtures is essential for optimizing the energy balance in high-energy-density systems. In this paper, we focus on one transport property, ion–ion temperature relaxation in a strongly coupled plasma mixture. We review the physics of temperature relaxation and derive a general temperature relaxation equation that includes dynamical correlations. We demonstrate the fidelity of three popular kinetic models that include only static correlations by comparing them to data from molecular dynamics simulations. We verify the simulations by comparing with laboratory data from ultracold neutral plasmas. By comparing our simulations with high fidelity kinetic models, we reveal the importance of dynamical correlations in collisional relaxation processes. These correlations become increasingly significant as the ion mass ratio in a binary mixture approaches unity.

I. INTRODUCTION

Plasma mixtures are ubiquitous in high energy-density (HED) science. At high density and temperature, ions are often assumed to be completely mixed and thermalized.[1] However, this is not necessarily the case. Persistent non-equilibrium separations in physical or velocity space have been observed.[2,3] The kinetics of these systems, including temperature relaxation, continues to be an ongoing area of research.[4–8]

We recently demonstrated a table-top experiment that generates non-equilibrium two-temperature ion mixtures[9–11] that are ideal for probing temperature relaxation in strongly coupled binary plasmas. The plasmas are generated by photoionizing laser-cooled Ca and Yb atoms to form a dual-species ultracold neutral plasma (UNP). The ion velocity distributions are determined using precision laser spectroscopy. After ionization, the Yb^+ and Ca^+ ions separately form Maxwellian velocity distributions. These gradually relax toward a single temperature before the plasma expands.

Well known processes in one-component plasmas are less clearly understood in mixtures. In a one-component plasma, relaxation phenomena demonstrate a separation of time scales with fast correlational processes, followed by slower kinetic processes, followed by even slower hydrodynamic behavior,

$$\tau_c \ll \tau_k \ll \tau_h. \tag{1}$$

The shortest of these time scales, τ_c, involves multiparticle processes which relax the multiparticle distribution $f_N(\mathbf{r}_1, \mathbf{r}_2, \ldots, \mathbf{v}_1, \mathbf{v}_2, \ldots; t)$ to a functional of the one-particle distribution function $f(\mathbf{r}, \mathbf{v}; t)$. The equations governing this regime are the Bogoliubov–Born–Green–Kirkwood–Yvon hierarchy. In a one-component plasma τ_c is proportional to the inverse of the ion plasma frequency. In single species UNP experiments, the inverse of the ion plasma frequency is on the order of a few hundred ns. In HED Physics (HEDP) experiments, it decreases to an order of one fs.

The timescale τ_k involves kinetic processes which relax the one-particle distribution function to its equilibrium value. These processes are described by kinetic equations, such as the Boltzmann equation or the Lenard–Balescu equation, where the primary quantity is the one-particle distribution function, $f(\mathbf{r}, \mathbf{v}; t)$. In a plasma, this timescale is associated with the inverse of the collision frequency.

The longest timescale, τ_h, corresponds to hydrodynamic processes in which only a small number of moments of $f(\mathbf{r}, \mathbf{v}; t)$ are evolved to determine thermodynamic variables. In this regime, macroscopic quantities relax to their equilibrium values. In single species UNP experiments, this time is on the order of a few μs, while in HEDP experiments, it is on the order of 1 ns.

In binary mixtures, the hierarchy in Eq. (1) is not valid when the mass ratio approaches unity. For example, in a binary mixture of electrons and ion, electron–electron collision processes (characterized by τ_{ee}) are faster than ion–ion collision processes (characterized by τ_{ii}), and both of these are much faster than electron–ion collision processes (characterized by τ_{ei})

$$\tau_{ee} \ll \tau_{ii} \ll \tau_{ei}. \tag{2}$$

However, these time scales depend on mass. The ratios of these timescales is

$$\frac{\tau_{ii}}{\tau_{ee}} \sim \sqrt{\frac{m_i}{m_e}} < \frac{\tau_{ei}}{\tau_{ee}} \sim \frac{m_i}{m_e}. \tag{3}$$

We extend this idea to binary mixtures of ions by replacing "electron" in the previous sentences with "low-mass ion." Obviously, from Eq. (3), when the ion mass ratio approaches unity, the timescale ratio also approaches unity and the hierarchy of Eq. (1) is broken. Dynamical correlations between the particles, important during τ_c and τ_k, need to be included in theoretical models.

Dual species UNPs provide a platform for studying temperature relaxation and other transport properties in a two temperature ionic mixture. In the present work, we use Ca and Yb atoms, with a mass ratio near 0.25. This study extends and complements electron–ion temperature relaxation work in which Eq. (3) was assumed. We use Molecular Dynamics (MD) studies to probe the influence of coupled modes on temperature relaxation. Time-evolving velocity distributions are obtained for six different ionic mixtures: H–Yb, Be–Yb, Mg–Yb, Ca–Yb, Sr–Yb, Nd–Yb. These ionic mixtures probe a density ratio from 0.006 to 0.83. The MD temperature relaxation rates are compared to theoretical predictions. These theories exclude dynamical correlations by design. The comparison of MD to theory provides a coupled-mode correction to the theory.

This paper is a continuation of our work presented in Ref. 11. In there we performed experiments and MD simulations for a Ca–Yb mixture for different concentrations. We compared those results with three common theoretical models and indicated that their failures arise from the lack of consideration of dynamical correlations. In this paper, we extend that work by providing a complete theoretical framework that includes dynamical correlations. We also present MD simulations for mixtures with different mass ratios. Some discussion and results of Ref. 11 we will be reproduced here for clarity. In Sec. II of this paper, we present the three temperature relaxation models that will be compared. In Sec. III we derive temperature relaxation equation from first principles with reference to the timescale discussion mentioned above. A similar derivation can be found in Ref. 12. In Secs. IV and V, we present the experimental setup and molecular dynamics simulations. Results are presented and discussed in Sec. VI.

II. MODELS

This discussion was previously presented in Ref. 11. We consider a spatially homogeneous plasma composed of two ion species with different masses, m_α, different number densities, n_α, and charge numbers, Z_α. The surrounding negative electronic background is at temperature T_e and density $n_e = Z_1 n_1 + Z_2 n_2$. The Wigner–Seitz radius is defined from the total ion number density, $a_{ws}^3 = 3/4\pi n_{tot}$, $n_{tot} = n_1 + n_2$. The concentration of each ion species is $x_\alpha = n_\alpha/n_{tot}$. Notice that $n_e = n_{tot}$ when $Z_1 = Z_2 = 1$. The ion Debye length of species α is $\lambda_\alpha^2 = \epsilon_0 k_B T_\alpha/(n_\alpha (Z_\alpha e)^2)$. The ion plasma frequency of species α is $\omega_\alpha^2 = (Z_\alpha e)^2 n_\alpha/(\epsilon_0 m_\alpha)$. The total ion plasma frequency is $\omega_p^2 = \sum_\alpha \omega_\alpha^2$. We further define an average temperature as

$$T_{avg} = \frac{m_\alpha T_\beta + m_\beta T_\alpha}{m_\alpha + m_\beta}, \tag{4}$$

and the ion thermal speed of species α is given by $v_{\alpha,th} = \sqrt{k_B T_\alpha/m_\alpha}$. The coupling plasma parameter of species α is defined as

$$\Gamma_\alpha = \frac{(Z_\alpha e)^2}{4\pi\epsilon_0 a_{ws}} \frac{1}{k_B T_\alpha}. \tag{5}$$

Typical equilibrium values in our experiments are $\Gamma_\alpha = 3$.

In a spatially homogeneous plasma with two ion species, collisional temperature relaxation[13] is described as

$$\frac{dT_\alpha}{dt} = -\nu_{\alpha\beta}(T_\alpha - T_\beta), \tag{6}$$

where α, β refer to different ion species. The collision frequency $\nu_{\alpha\beta}$ depends critically on temperature, density, and charge. In general, the collision frequencies can be represented as

$$\nu_{\alpha\beta} = n_\beta \Phi \mathcal{S}, \tag{7}$$

where

$$\Phi = \left(\frac{Z_\alpha Z_\beta e^2}{4\pi\epsilon_0}\right)^2 \frac{\sqrt{m_\alpha m_\beta}}{(m_\alpha + m_\beta)^{3/2}} \left(\frac{1}{k_B T_{avg}}\right)^{3/2} \tag{8}$$

and $\mathcal{S}$ is a model-dependent collisional integral.

Most treatments of temperature relaxation focus on electron–ion systems with the electron temperature much higher than the ion temperature. Few of these theoretical results can be applied directly to the case of ion–ion relaxation when the mass ratio is near unity. However, in the following, we discuss ion–ion temperature relaxation rates derived from three models with increasing fidelity.

The first model is found in the Naval Research Laboratory (NRL) Plasma Formulary,[14] p. 33. This model is based on the Fokker–Planck equation that leads to the well-known Coulomb logarithm. In strongly coupled plasmas, $\mathcal{S}$ is negative and needs to be modified.

A treatment based on hyperbolic trajectories[15] yields a positive definite result and takes the form

$$\mathcal{S}^{NRL} = \frac{1}{2}\ln\left[1 + \left(\frac{b_{max}}{b_{min}}\right)^2\right], \tag{9}$$

where

$$b_{max} = \left(\frac{1}{\lambda_1^2} + \frac{1}{\lambda_2^2}\right)^{-1/2}, \tag{10}$$

$$b_{min} = \left(\frac{Z_1 Z_2 e^2}{4\pi\epsilon_0}\right) \frac{1}{k_B T_{avg}}. \tag{11}$$

Equation (9) gives the NRL result in the limit of large values of the Coulomb logarithm.

The second model improves on the NRL by generalizing the approach of Gericke, Murillo, and Schangles (GMS) in Ref. 15 to ion–-ion collisions. Note that Eq. (10) tends to zero at low temperatures and

does not include electron screening. This needs to be repaired for collision between screened strongly coupled ions. Choosing $b_{\max} = \lambda_{\text{eff}}$,

$$\lambda_{\text{eff}} = \left[\frac{1}{\lambda_{\text{TF}}^2} + \sum_{\alpha=1}^{2} \frac{1}{\lambda_\alpha^2 + a_{\text{ws}}^2/x_\alpha}\right]^{-1/2}, \tag{12}$$

addresses this problem.[4] The parameter λ_{TF} is the Thomas–Fermi length calculated from the electron temperature, T_e, and density, n_e, see Eq. (23) in Ref. 4. Note that Eq. (12) gives a positive definite value even at zero temperature. Finally, the GMS collision frequency appropriate for strongly coupled plasmas is

$$\nu_{ij}^{\text{GMS}} = n_j \Phi \mathcal{S}^{\text{GMS}}, \tag{13}$$

$$\mathcal{S}^{\text{GMS}} = \frac{1}{2}\ln\left[1 + \left(\frac{2\lambda_{\text{eff}}}{b_{\min}}\right)^2\right]. \tag{14}$$

The third model, referred to as Stanton Murillo Transport (SMT), is presented in detail in Ref. 13, and it is based on a multispecies Bhatnagar–Gross–Krook solution of the Boltzmann equation. The main difference from the NRL and GMS models is that the collisional integral is calculated numerically using a Yukawa interaction, instead of a bare Coulomb interaction, and without any assumption of weak-scattering.[4] This leads to a collisional frequency given by

$$\nu_{ij}^{\text{SMT}} = n_j \Phi \mathcal{S}^{\text{SMT}}, \tag{15}$$

$$\mathcal{S}^{\text{SMT}} = \frac{128}{3}\frac{\sqrt{\pi}}{2^{3/2}}\mathcal{K}_{11}(g), \tag{16}$$

where g is the thermally averaged ion–ion Coulomb coupling factor,

$$g = \left(\frac{Z_1 Z_2 e^2}{4\pi\epsilon_0}\right)\frac{1}{k_B T_{\text{avg}}}\frac{1}{\lambda_{\text{eff}}}. \tag{17}$$

Typical values in our experiments are $g \sim 0.5$. The collision integral $\mathcal{K}_{11}(g)$ is calculated from Eqs. (C22)–(C24) in Appendix C of Ref. 4.

III. DYNAMICAL CORRELATIONS

In general, the effective interaction between the two ion species is time and frequency dependent. The three models described above neglect the frequency dependence of the effective interaction and consider only the static case.[16–19] This effective interaction is then used to inform the Coulomb logarithm in a Fokker–Planck approach (NRL, GMS) or the cross section in a Boltzmann equation (SMT).

In this section, we present a derivation of the temperature relaxation equation starting from a microscopic description of the system. We indicate the points in which our derivation differs from previous work.[12,20,21] Our final result is Eq. (55), and it is obtained without the use of large mass ratio approximations.

Following the notation and convention of Ref. 12, we define the Fourier components of any observable as

$$A(\mathbf{r}t;\mathbf{v}) = \sum_{\mathbf{k}}\int_{-\infty}^{\infty}\frac{d\omega}{2\pi}A(\mathbf{k}\omega;\mathbf{v})e^{i(\mathbf{k}\cdot\mathbf{r}-\omega t)}, \tag{18}$$

$$A(\mathbf{k}\omega;\mathbf{v}) = \frac{1}{V}\int_V d\mathbf{r}\int_{-\infty}^{\infty}dt A(\mathbf{r}t;\mathbf{v})e^{-i(\mathbf{k}\cdot\mathbf{r}-\omega t)}. \tag{19}$$

We consider a multispecies plasma composed of $N = N_1 + N_2$ ionic species and $N_e = \sum_\alpha Z_\alpha N_\alpha$ electrons. The Hamiltonian of the system can be divided into three components,

$$\mathcal{H} = \mathcal{H}_e + \mathcal{H}_i + \mathcal{U}_{ei}, \tag{20}$$

where $\mathcal{U}_{ei}$ is the interaction between electrons and ions, and $\mathcal{H}_\sigma = \mathcal{T}_\sigma + \mathcal{U}_\sigma$ is the Hamiltonian of the σ subsystem, with $\mathcal{T}_\sigma$ being the kinetic energy and $\mathcal{U}_\sigma$ the interaction potential between the particles. For simplicity, we assume the absence of any external forces. The subscript σ will indicate both electrons and ions species.

The microscopic phase-space distribution of species σ is defined by

$$\mathcal{N}_\sigma(\mathbf{X};t) = \sum_i \delta[\mathbf{r} - \mathbf{r}_i(t)]\delta[\mathbf{p} - \mathbf{p}_i(t)], \tag{21}$$

where $\mathbf{X} = \{\mathbf{r}, \mathbf{p}\}$ is the set of positions and momenta. This distribution evolves in phase-space according to the Klimontovich equation,

$$\left[\frac{\partial}{\partial t} + \dot{\mathbf{r}}\cdot\frac{\partial}{\partial \mathbf{r}} + \dot{\mathbf{p}}\cdot\frac{\partial}{\partial \mathbf{p}}\right]\mathcal{N}_\sigma(\mathbf{X};t) = 0, \tag{22}$$

where

$$\dot{\mathbf{r}} = \frac{\partial \mathcal{H}}{\partial \mathbf{p}}, \quad \dot{\mathbf{p}} = -\frac{\partial \mathcal{H}}{\partial \mathbf{r}}. \tag{23}$$

Microscopic current and charge densities are then calculated via integration over velocity space,

$$\mathbf{J}(\mathbf{r},t) = \sum_\sigma Z_\sigma e\int d\mathbf{p}\,\frac{\mathbf{p}}{m_\sigma}\mathcal{N}_\sigma(\mathbf{X};t), \tag{24}$$

$$\rho(\mathbf{r},t) = \sum_\sigma Z_\sigma e n_\sigma(\mathbf{r},t), \tag{25}$$

$$n_\sigma(\mathbf{r},t) = \int d\mathbf{p}\mathcal{N}_\sigma(\mathbf{X};t). \tag{26}$$

Note that the sum $\sum_\sigma$ includes also the electrons with $Z_e = -1$.

The first step is to perform an ensemble average over the initial conditions of the system to obtain a continuum description of the system. It is important to note that this coarse-graining is not equivalent to a time average over correlation times $t \gg \tau_c$ as presented in Chapter 7 of Ref. 12. This ensemble average is meant only to remove the discreteness of $\mathcal{N}_\sigma(\mathbf{X};t)$, and it is an average over the Liouville distribution, as defined in Chapter 2 B of Ref. 12. Denoting this average by $\langle\ldots\rangle$, we expand $\mathcal{N}_\sigma(\mathbf{X};t)$ as

$$\mathcal{N}_\sigma(\mathbf{X};t) = f_\sigma(\mathbf{X};t) + \delta N_\sigma(\mathbf{X},t), \tag{27}$$

where $f_\sigma(\mathbf{X};t) = \langle\mathcal{N}_\sigma(\mathbf{X};t)\rangle$ is the ensemble average, and $\delta N_\sigma(\mathbf{X};t)$ are the fluctuations due to the discreteness of $\mathcal{N}_\sigma(\mathbf{X};t)$. Such coarse-graining, in the absence of external fields, and with $\mathbf{v} = \mathbf{p}/\mathbf{m}$, leads to

$$\left[\frac{\partial}{\partial t} + \mathbf{v}\cdot\frac{\partial}{\partial \mathbf{r}}\right]f_\sigma = -\frac{\partial}{\partial \mathbf{p}}\langle\delta\mathcal{N}_\sigma\delta\mathbf{F}_\sigma\rangle \tag{28}$$

and

$$\left[\frac{\partial}{\partial t} + \mathbf{v}\cdot\frac{\partial}{\partial \mathbf{r}}\right]\delta\mathcal{N}_\sigma = \mathcal{C}(\mathbf{X},t), \tag{29}$$

$$\mathcal{C}(\mathbf{X},t) = -\delta\mathbf{F}_\sigma \cdot \frac{\partial}{\partial \mathbf{p}}\left(f_\sigma + \delta\mathcal{N}_\sigma\right). \tag{30}$$

The term $\delta\mathbf{F}_\sigma = \sum_{\sigma'} \delta\mathbf{F}_{\sigma\sigma'} = \delta\mathbf{F}_{\sigma e} + \sum_\alpha \delta\mathbf{F}_{\sigma\alpha}$ is the fluctuation in the force field, experienced by particles of species σ, due to all other particles.

Hydrodynamic quantities are then calculated by averaging Eq. (28) over different moments of the momenta. In this paper, we are interested in the temperature that we define as

$$\frac{3}{2} n_\sigma k_B T_\sigma(\mathbf{r},t) = \int d\mathbf{p}\, \frac{|\mathbf{p}|^2}{2m_\sigma} f_\sigma(\mathbf{X},t). \tag{31}$$

Multiplying Eq. (28) by $|\mathbf{p}|^2/(2m_\sigma)$ and integrating over the momenta, we arrive at

$$\frac{dT_\sigma}{dt} + \frac{\partial}{\partial \mathbf{r}} \cdot \mathbf{Q}_\sigma(\mathbf{r},t) = \frac{1}{3n_\sigma k_B} \langle \delta\mathbf{j}_\sigma(\mathbf{r},t) \cdot \delta\mathbf{F}_\sigma(\mathbf{r},t)\rangle, \tag{32}$$

where

$$\mathbf{Q}_\sigma = \frac{1}{3n_\sigma k_B} \int d\mathbf{p}\, \frac{|\mathbf{p}|^2}{m_\sigma} \mathbf{v} f_\sigma(\mathbf{X},t) \tag{33}$$

is a heat flux and $\delta\mathbf{j}_\sigma(\mathbf{r},t) = \int d\mathbf{p}\, \mathbf{v}\delta N_\sigma(\mathbf{X};t)$ is the fluctuation of the microscopic density current of species σ. Since we are considering a homogeneous plasma with no net heat flux, we can neglect the second term and write

$$\frac{dT_\sigma}{dt} = \frac{1}{3n_\sigma k_B} \langle \delta\mathbf{j}_\sigma(\mathbf{r},t) \cdot \delta\mathbf{F}_\sigma(\mathbf{r},t)\rangle. \tag{34}$$

This equation is somewhat different than those in Refs. 22 and 23 due to our definitions of current density and the Fourier transform.

At this point, it is important to note the timescales over which each of the terms in Eq. (34) evolves. It is often assumed that the left-hand side (LHS) of the equation involves slow processes that can be assumed constant over a timescale τ. Therefore, we perform an average over timescales $\tau \ll t, \tau_k$, such that

$$\frac{1}{\tau}\int_0^\tau ds \frac{dT_\sigma}{dt} \approx \frac{dT_\sigma}{dt}. \tag{35}$$

Such averaging though should be taken carefully on the right-hand side (RHS) since $\delta\mathbf{j}_\sigma(\mathbf{r},t)$ and $\delta\mathbf{F}_\sigma(\mathbf{r},t)$ are microscopic fluctuations that contain information about intra-species collision processes, $\tau_{\sigma\sigma}$, and inter-species collision processes $\tau_{\sigma\sigma'}$, that are proportional to τ. Changing to Fourier space in the RHS of Eq. (34), we have

$$\begin{aligned}\frac{1}{\tau}\int_0^\tau ds \langle \delta\mathbf{j}_\sigma(\mathbf{r},s) \cdot \delta\mathbf{F}_\sigma(\mathbf{r},s)\rangle \\ = \frac{1}{\tau}\int_0^\tau ds \int\int \frac{d\omega}{2\pi}\frac{d\omega'}{2\pi} \langle \delta\mathbf{j}_\sigma(\mathbf{r}\omega) \cdot \delta\mathbf{F}_\sigma(\mathbf{r}\omega')\rangle e^{-i(\omega+\omega')s}.\end{aligned} \tag{36}$$

The timescale, t, of the LHS is much longer than τ such that it allows us to effectively take the limit $\tau \to \infty$ and obtain a Dirac delta from the integral over s. That is,

$$\begin{aligned}\lim_{\tau\to\infty}\frac{1}{\tau}\int_0^\tau ds \langle \delta\mathbf{j}_\sigma(\mathbf{r},s) \cdot \delta\mathbf{F}_\sigma(\mathbf{r},s)\rangle \\ = \sum_{\mathbf{k}} \int \frac{d\omega}{2\pi} \langle \delta\mathbf{j}_\sigma(-\mathbf{k}-\omega) \cdot \delta\mathbf{F}_\sigma(\mathbf{k}\omega)\rangle,\end{aligned} \tag{37}$$

where we have omitted a similar argument over length scales and moved to $\mathbf{k}$ space. This averaging process is crucial because it defines transport coefficients derived from the hydrodynamic equations and links them to microscopic processes via Green–Kubo relations.

The derivation continues by connecting the microscopic current density and force fluctuations to density fluctuations, the former via the continuity equation,

$$\delta\mathbf{j}_\sigma(\mathbf{k}\omega) = \frac{\omega}{k^2}\mathbf{k}\,\delta n_\sigma(\mathbf{k}\omega), \tag{38}$$

and the latter via the gradient of an interacting potential $U_{\sigma\sigma'}$,

$$\delta\mathbf{F}_\sigma(\mathbf{k}\omega) = i\mathbf{k}\sum_{\sigma'\neq\sigma} U_{\sigma\sigma'}(\mathbf{k}\omega)\delta n_{\sigma'}(\mathbf{k}\omega), \tag{39}$$

with $\delta n_\sigma(\mathbf{k}\omega) = \int d\mathbf{p}\delta\mathcal{N}_\sigma(\mathbf{k}\omega)$. Substituting the above equations in Eq. (32), we obtain

$$\frac{dT_\sigma}{dt} = \frac{1}{3n_\sigma k_B}\sum_{\sigma'\neq\sigma}\sum_{\mathbf{k}}\int\frac{d\omega}{2\pi}\omega U_{\sigma\sigma'}(\mathbf{k}\omega)\mathrm{Im}\langle\delta n_\sigma^*(\mathbf{k}\omega)\delta n_{\sigma'}(\mathbf{k}\omega)\rangle, \tag{40}$$

where $\delta n_\sigma^*(\mathbf{k}\omega) = \delta n_\sigma(-\mathbf{k}-\omega)$.

We stress that this derivation involved two averaging procedures at two different stages. The first is an ensemble average needed for a continuum description of the systems. The second is a time average over fast microscopic processes that evolve on a timescale much shorter than macroscopic quantities that appear in the LHS of Eq. (34). Furthermore, we note that we have not made use of the mass difference between the species and only noted the existence of inter-species, $\tau_{\sigma\sigma'}$, and intra-species, $\tau_{\sigma\sigma}$, timescales. The effects of such assumption will be considered further in the discussion.

Finally, we conclude this section by defining several systems: an e–i plasma, a multicomponent e–i plasma, a Binary Ionic Mixture (BIM), and a Binary Yukawa Mixture (BYM).

The former is a two component system with only one ion species and one electron species. The particles interact via the bare Coulomb potential,

$$U_{\sigma\sigma'}(\mathbf{k}\omega) = U_{ei}(k) = -\frac{Z_i e^2}{\epsilon_0}\frac{1}{k^2}. \tag{41}$$

In the case of a plasma with multiple ion species and electrons where all the species are dynamical, we refer to it as a multicomponent e–i plasma.

A BIM is a two component plasma composed of two ion species interacting via the bare Coulomb potential. The electrons form a static background that provides stability to the system and do not interact with ions. The ions interact via the potential

$$U^{(\mathrm{BIM})}_{\sigma\sigma'}(\mathbf{k}\omega) = U^{(\mathrm{BIM})}_{12}(k) = \frac{Z_1 Z_2 e^2}{\epsilon_0}\frac{1}{k^2}. \tag{42}$$

A BYM is a plasma composed of two ion species that interact via a screened Coulomb or Yukawa potential. The electrons form a polarizable background responsible for the screening. This interaction can be derived by considering the large mass difference between electrons and ions. This allows us to make use of the Born-approximation, that

is we can integrate out the degrees of freedom of the electrons. This translates in an effective Hamiltonian for the ions,

$$\mathcal{H}_I = \mathcal{T}_I + \mathcal{U}_I + \mathcal{F}_{ei} = \mathcal{T}_I + U_I, \tag{43}$$

where $U_I = \mathcal{U}_I + \mathcal{F}_{ei}$ and $\mathcal{F}_{ei}$ is the total free energy of all terms that involve the electrons. This is the effective Hamiltonian used in ionic MD. A detailed derivation of the ion–ion interacting potential, considering different properties of the electron liquid, is presented in Ref. 24. For BYM under investigation here, the two ion species interact via a binary Yukawa potential of the form

$$U^{(\mathrm{BYM})}_{\sigma\sigma'}(\mathbf{k}\omega) = U^{(\mathrm{BYM})}_{12}(k) = \frac{Z_1 Z_2 e^2}{\epsilon_0}\frac{1}{k^2 + \lambda_{TF}^{-2}}. \tag{44}$$

In the following, we continue our derivation by considering a multicomponent e–i plasma with electrons and two ions species. The e–i plasma, BIM, and BYM cases will be considered in Secs. III B and III C.

A. Density correlations

Returning to Eq. (40), in order to make further progress, we need to relate the correlations of $\delta n_\sigma(\mathbf{k}\omega)$ to computable quantities. We thus look for a solution to Eqs. (29) and (30). The general form of a solution is

$$\delta n_\sigma(\mathbf{k}\omega) = \delta n^{(0)}_\sigma(\mathbf{k}\omega) + \delta n^{(\mathrm{ind})}_\sigma(\mathbf{k}\omega), \tag{45}$$

where the first term, $\delta n^{(0)}_\sigma$, often referred to as spontaneous fluctuations, is the solution of the homogeneous equation, and $\delta n^{(\mathrm{ind})}_\sigma$ is obtained from a recursive solution.

The homogeneous equation,

$$\left[\frac{\partial}{\partial t} + \mathbf{v}\cdot\frac{\partial}{\partial \mathbf{r}}\right]\delta N^{(0)}_\sigma = 0, \tag{46}$$

represents the fluctuation of a non-interacting gas of particles and it is readily available, see Eq. (7.27) of Ref. 12.

The term $\delta n^{(\mathrm{ind})}_\sigma$ can be related to $\delta n^{(0)}_\sigma$ via linear response theory as

$$\delta n^{(\mathrm{ind})}_\sigma(\mathbf{k}\omega) = \sum_{\sigma'} U_{\sigma\sigma'}\Pi_{\sigma\sigma'}(\mathbf{k}\omega)\delta n^{(0)}_{\sigma'}(\mathbf{k}\omega), \tag{47}$$

where

$$\Pi_{\sigma\sigma'}(\mathbf{k}\omega) = \chi^{(0)}_\sigma(\mathbf{k}\omega)[1 - G_{\sigma\sigma'}(\mathbf{k}\omega)] \tag{48}$$

are the elements of the matrix $\Pi(\mathbf{k}\omega)$ defined from the free particle polarizability, $\chi^{(0)}_\sigma(\mathbf{k}\omega)$, and local field correction, $G_{\sigma\sigma'}(\mathbf{k}\omega)$. Defining as η the inverse of the matrix $A(\mathbf{k}\omega) = \mathbf{I} - U\Pi(\mathbf{k}\omega)$, we arrive at[12,22]

$$\delta n_\sigma(\mathbf{k}\omega) = \sum_{\sigma'}\eta_{\sigma\sigma'}(\mathbf{k}\omega)\delta n^{(0)}_{\sigma'}(\mathbf{k}\omega). \tag{49}$$

It is convenient, for the following discussion, to write equations for one ion species only, say 1. Equations for electrons and species 2 are obtained via the exchange $1 \to e$ or $1 \to 2$. The correlation functions become

$$\langle \delta n^*_1(\mathbf{k}\omega)\delta n_2(\mathbf{k}\omega)\rangle = \sum_\sigma \eta^*_{1\sigma}\eta_{2\sigma}\langle(\delta n^{(0)}_\sigma)^*\delta n^{(0)}_\sigma\rangle, \tag{50}$$

where the cross terms, $\langle(\delta n^{(0)}_\sigma)^*\delta n^{(0)}_{\sigma'}\rangle$, are identically zero since they represent correlations between two ideal plasmas.

Finally, the ensemble averages can now be related to computable quantities via the fluctuation-dissipation theorem,

$$\langle(\delta n^{(0)}_\alpha)^*(\mathbf{k}\omega)\delta n^{(0)}_\beta(\mathbf{k}\omega)\rangle = \frac{(2\pi)^2}{V}\delta_{\alpha\beta}S_{\alpha\beta}(\mathbf{k}\omega), \tag{51}$$

$$S^{(0)}_{\alpha\beta}(\mathbf{k}\omega) = -\frac{k_B T_\alpha}{\pi\omega}\mathrm{Im}\hat{\chi}^{(0)}_{\alpha\beta}(\mathbf{k}\omega), \tag{52}$$

where $\hat{\chi}^{(0)}_{\alpha\beta}(\mathbf{k}\omega)$ is the external response function. Changing the sum of $\mathbf{k}$ to an integral

$$\sum_{\mathbf{k}} \to \frac{V}{(2\pi)^3}\int dk k^2(4\pi), \tag{53}$$

the temperature relaxation equation becomes

$$\frac{dT_\sigma}{dt} = \int\int \frac{dk\,d\omega}{3n_1\pi^3}\,k^2\sum_{\sigma'\neq\sigma}U_{\sigma\sigma'}\left\{\sum_\alpha \mathrm{Im}\left[\eta^*_{\sigma\alpha}\eta_{\sigma'\alpha}\right]T_\alpha\mathrm{Im}\hat{\chi}^{(0)}_\alpha\right\}, \tag{54}$$

which written explicitly for species 1 is

$$\begin{aligned}\frac{dT_1}{dt} = \int\int \frac{dk\,d\omega}{3n_1\pi^3}\frac{k^2}{|\varepsilon(\mathbf{k}\omega)|^2}\{&T_1\big(U_{12}\mathrm{Im}\left[\tilde{\eta}^*_{1,1}\tilde{\eta}_{2,1}\right] \\ &+U_{1e}\mathrm{Im}\left[\tilde{\eta}^*_{1,1}\tilde{\eta}_{e,1}\right]\big)\mathrm{Im}\hat{\chi}^{(0)}_{11} + T_2\big(U_{12}\mathrm{Im}\left[\tilde{\eta}^*_{1,2}\tilde{\eta}_{2,2}\right] \\ &+U_{1e}\mathrm{Im}\left[\tilde{\eta}^*_{1,2}\tilde{\eta}_{e,2}\right]\big)\mathrm{Im}\hat{\chi}^{(0)}_{22} + T_e\big(U_{12}\mathrm{Im}\left[\tilde{\eta}^*_{1,e}\tilde{\eta}_{2,e}\right] \\ &+U_{1e}\mathrm{Im}\left[\tilde{\eta}^*_{1,e}\tilde{\eta}_{e,e}\right]\big)\mathrm{Im}\hat{\chi}^{(0)}_{ee}\Big\}.\end{aligned} \tag{55}$$

The denominator $|\varepsilon(\mathbf{k}\omega)|$ is the absolute value of the determinant of the A matrix and none other than the dielectric function, and $\tilde{\eta}_{\alpha,\beta}$ is the (α,β)-cofactor of the A matrix. We recall that in this case $\varepsilon(\mathbf{k}\omega)$ is the dielectric function of a three component plasma, two ion species, and the electrons. Equation (55) and its counterpart for species 2 and the electrons are the general formulas for thermal relaxation in a classical BIM.

The static limit of Eq. (55) is obtained by writing $\varepsilon(\mathbf{k}\omega) = 1 + [\lambda_1^{-2} + \lambda_2^{-2} + \lambda_e^{-2}]/k^2$. This fully static approach was used in SMT. However, they used velocity dependent cross sections to explore the importance of dynamical ion screening in an e–i plasma. In general, they found the dynamical correction to viscosity and self-diffusion to be small, see Sec. VI in Ref. 4. As we argue here, the dynamical effects are large for BYMs and depend on the ions mass and density ratios.

B. e–i Plasma

In the case of an e–i plasma, as considered in Refs. 12, 21, 22, and 25, all the terms with subscript 2 disappear and Eq. (55) simplifies to

$$\begin{aligned}\frac{dT_i}{dt} = \int\int \frac{dk\,d\omega}{3n_1\pi^3}\,k^2&\left(\frac{U_{ie}(\mathbf{k}\omega)}{|\varepsilon(\mathbf{k}\omega)|}\right)^2 \\ &\times\left\{T_i\mathrm{Im}\left[\Pi_{ei}A^*_{ee}\right]\mathrm{Im}\hat{\chi}^{(0)}_{ii} - T_e\mathrm{Im}\left[\Pi^*_{ie}A_{ii}\right]\mathrm{Im}\hat{\chi}^{(0)}_{ee}\right\},\end{aligned} \tag{56}$$

with U_{ei} given by Eq. (41) and the dielectric function contains both the ion and electron response functions. Further simplification is achieved,

in the weak coupling regime ($G_{\sigma\sigma'} = 0$), by considering the large mass difference between electrons and ions. One then arrives at the well-known Landau–Spitzer formula for the electron–ion collision frequency and to a temperature relaxation equation of the form of Eq. (6).[12,21,25] The work presented in Refs. 20, 21, and 25, instead, addresses the strong coupling regime.

C. BIM and BYM

In the case of BIM and BYM, the electron terms vanish and one arrives at

$$\frac{dT_1}{dt} = \int\int \frac{dk\, d\omega}{3n_1\pi^3}\, k^2 \left(\frac{U_{12}(\mathbf{k}\omega)}{|\varepsilon(\mathbf{k}\omega)|}\right)^2 \times \left\{T_1 \mathrm{Im}\left[\Pi_{21}A_{22}^*\right]\mathrm{Im}\hat{\chi}_{11}^{(0)} - T_2 \mathrm{Im}\left[\Pi_{12}^* A_{11}\right]\mathrm{Im}\hat{\chi}_{22}^{(0)}\right\}, \quad (57)$$

and its counterpart for species 2. The interaction potential U_{12} is given by Eq. (42) for BIM and by Eq. (44) for BYM. The dielectric function $\varepsilon(\mathbf{k}\omega)$ contains only the ions' response functions and not the electronic response. When the mass ratio between ions is close to unity, no further simplification is possible and we cannot move forward without a strong coupling theory.

The two most likely candidates for a strong coupling theory are the dynamical local field correction[12] and the Quasi-Localized Charge Approximation (QLCA).[26] While several static approximations for the LFC have been used for e–i plasmas,[21,25] no dynamical extension has been performed to binary ionic mixtures. The QLCA, on the other hand, has proven successful in predicting the collective mode spectrum of both a BIM[27] and BYM.[28,29] The collective modes are the frequencies for which $|\varepsilon(\mathbf{k}\omega)| = 0$; thus, they will be the primary contributors of the ω integral.

In a BIM, the QLCA predicts two plasmon modes as opposed to an e–i plasma where there is one plasmon mode, at $\omega_{p,e}$, and an ion-acoustic mode. In the case of BYM, however, an optic mode and an acoustic mode with a sound speed smaller than its weakly coupled counterpart are predicted.[27–31]

IV. EXPERIMENTS

Our measurement techniques and data analysis have been described in previous works.[9–11] We trap approximately 10×10^6 Ca and Yb atoms in a dual species magneto-optical trap (MOT). The neutral atom density is approximately spherically symmetric and Gaussian of the form $n(r) = n_0 \exp(-r^2/2\sigma_0^2)$ with $n_0 = 10^8$ to 10^{10} cm^{-3} and $\sigma_0 = 0.3$ to 1.0 mm. The neutral atom temperature is a few mK. The trapped neutral atoms are ionized using two color photo ionization as shown in Fig. 1. Laser pulses at 423 and 390 nm ionize Ca→Ca$^+$, and laser pulses at 399 and 394 nm laser pulses ionize Yb→Yb$^+$. The amount by which the ionizing laser photon energy exceeds the ionization threshold sets the electron temperature. Typical values for the electron temperature are 50 to 200 K.

Although the ions initially retain the mK temperatures of the neutral atom cloud, the ion velocity distributions rapidly broaden as individual ions respond to the sudden appearance of neighboring ions.[32] This disorder-induced heating (DIH) occurs because in the neutral atom cloud the atom pair distribution function is flat, $g(r) = 1$. As the ions push neighboring ions away, excess electrical potential energy is converted to kinetic energy and the ion temperature rises to values near 1 K.[33]

After ionization, we probe the ion velocity distributions using laser-induced fluorescence on strongly allowed transitions at $\lambda = 393$ and 369 nm (see Fig. 1). The frequency of the probe laser beams is offset from the resonance transition frequency by a value Δf. The fluorescence signal is proportional to the number of ions Doppler shifted into

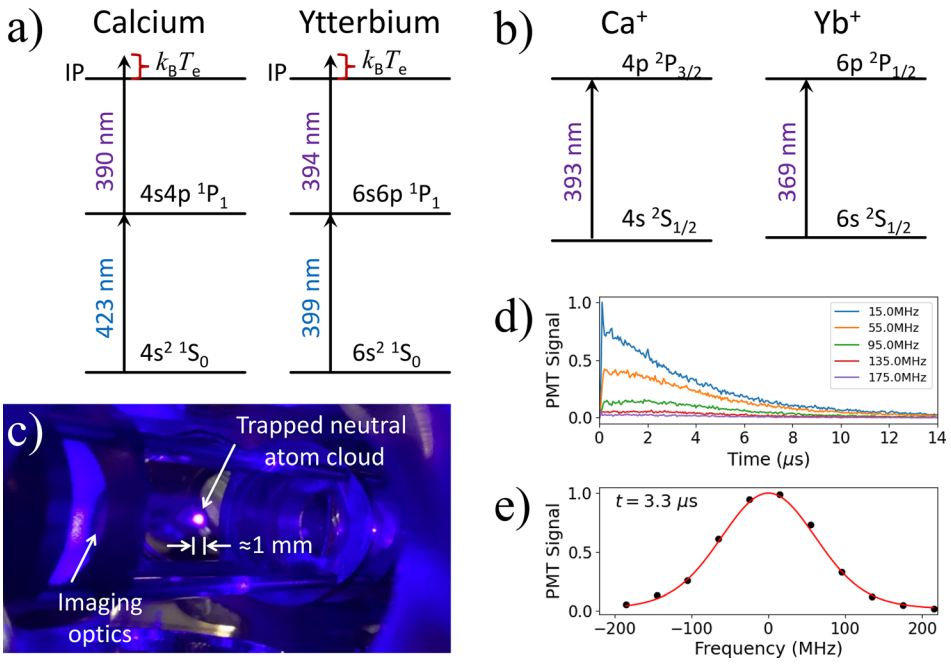

FIG. 1. Experimental details for the dual-species ultracold neutral plasma. (a) A partial energy level diagram for neutral Ca and Yb showing the laser cooling transitions at 423 and 399 nm and the ionization laser wavelengths. (b) The probe laser wavelengths and transitions used for laser-induced fluorescence measurements on plasma ions. (c) An image of the trapped neutral atom cloud. (d) Laser-induced fluorescence from Ca$^+$ ions in an expanding plasma. (e) Typical fluorescence data (black circles) and Voigt profile fit (red line) at $t = 3.3\ \mu$s.

resonance with the laser, with a velocity $v = \Delta f/\lambda$. By repeating the fluorescence measurements with Δf ranging from typically -150 to $+150$ MHz, we map out the ion velocity distribution. Due to the finite width of the atomic transitions, the fluorescence signal is a convolution of the atomic transition line shape with the ion velocity distribution. Accordingly, we fit the fluorescence signal at a given time after ionization to a Voigt profile (see Fig. 1) with the Gaussian width $f_{\rm rms} = (k_B T_i/m_i)^{1/2}/\lambda$ as a fit parameter. From the time-evolving Gaussian width, we obtain the ion temperature. Additional lasers are used in Ca^+ to prevent optical pumping into dark states. We verify that in our experimental conditions, optical pumping is negligible.

The calcium and ytterbium ion temperatures for two different plasma densities are shown in Figs. 2(a) and 2(b). The ion temperatures rapidly rise during the first 100 ns due to DIH, and the two ion species thermalize to their own post-DIH temperature before gradually approaching equilibrium. The two-temperature nature of this system arises naturally as a consequence of the unequal masses.[11] The ion temperature differences are plotted in Figs. 2(c) and 2(d). Also shown are results from an MD simulation, which we discuss in Sec. V.

V. MD SIMULATIONS

Molecular dynamics simulations are carried out using the Sarkas package, a pure python open-source molecular dynamics code for non-ideal plasma simulation.[34] The system is composed of two ion species whose particles interact via the Yukawa potential,

$$U(r_{\alpha\beta}) = \frac{Z_\alpha Z_\beta e^2}{4\pi\epsilon_0}\frac{1}{r_{\alpha\beta}} e^{-r_{\alpha\beta}/\lambda_{\rm TF}}, \tag{58}$$

where $\lambda_{\rm TF}$ is the Thomas–Fermi length of the electrons with density, n_e, and temperature, T_e. The initial positions of the ions are randomly distributed along the three axes of the simulation box. The initial velocities, however, are chosen from normal distribution with an initial width $v^{(0)}_{\alpha,\rm rms} = \sqrt{k_B T_0/m_\alpha}$ with $T_0 = 2$ mK.

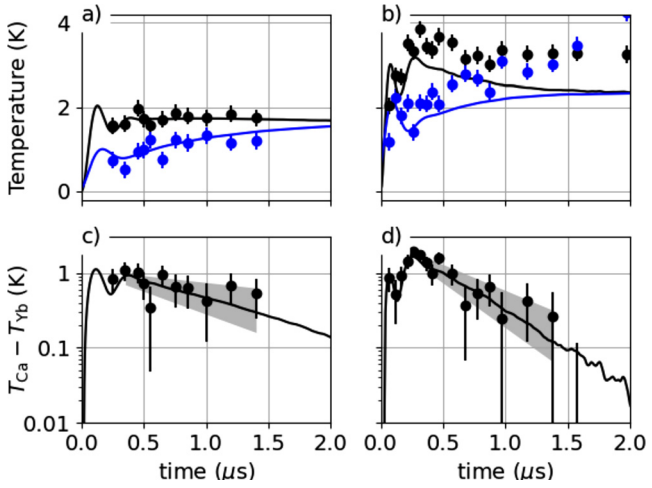

FIG. 2. Temperature vs time for two UNP configurations. (a) $T_{\rm Ca}$ (black), $n_0^{\rm Ca} = 3.4 \times 10^9$ cm^{-3}, $\sigma_0^{\rm Ca} = 0.57$ mm, and $T_{\rm Yb}$ (blue), $n_0^{\rm Yb} = 1.9 \times 10^9$ cm^{-3}, $\sigma_0^{\rm Yb} = 0.72$ mm. Circles show temperatures extracted from laboratory data. Solid lines show MD data as described in Sec. V. (c) Temperature difference, $T_{\rm Ca}$–$T_{\rm Yb}$. Circles show laboratory data. Solid lines show MD data. The gray shaded area represents the estimated $1-\sigma$ uncertainties in the decay rate extracted from the laboratory data. Panels (b) and (d) show the same analysis for a higher density plasma with $n_0^{\rm Ca} = 4.3 \times 10^9$ cm^{-3}, $\sigma_0^{\rm Ca} = 0.53$ mm, and $n_0^{\rm Yb} = 1.3 \times 10^{10}$ cm^{-3}, $\sigma_0^{\rm Yb} = 0.38$ mm. For all of these data, the electron temperature is 96 K.

Following the experimental parameters, in the first 40 ns of the simulation, Ca atoms are neutral, while Yb atoms carry a charge $Z = 1$. In this way, only the Yb^+ atoms interact with each other and do not interact with Ca atoms. For $t \geq 40$ ns, the charge number of Ca atoms is changed to 1 and the screening parameter $\kappa = a_{\rm ws}/\lambda_{\rm TF}$ is updated. Electron temperature and densities from the experiments lead to $\kappa \sim 0.37 - 0.46$. The potential energy and forces are calculated using a highly efficient Particle-Particle Particle-Mesh algorithm.[35] This algorithm is more reliable than the minimum image convention when κ is small.

MD simulations are performed for plasmas with a uniform spatial density, obtained from experimental values, and periodic boundary conditions. While the experiments necessarily have open boundary conditions, the MD simulations are an appropriate representation of the middle of the plasma, where the density gradient is small and the thermalization time is faster than the expansion time. For these initial conditions, there is no equilibration phase in the MD code. Particle positions and velocities are integrated using the standard velocity Verlet algorithm. The time step and total number of particles were varied and chosen to give converged results. In our simulations, we use $N = 50\,000$ total ions, with number ratios matching those of the experiments. The timesteps were chosen such that $\omega_p \Delta t \sim 0.002$. For each experiment, five MD non-equilibrium simulations with different initial conditions were performed.

VI. RESULTS

A detailed discussion of the cross validation of simulation and experiment is presented in Ref. 11. In that publication, we also discussed the failures of the three models and suggested the need to include dynamical correlations. In the following discussion, we explore the importance of dynamical correlations in more detail.

Full calculations of the integrals in Eq. (57) are not available without appealing to theoretical models for the dielectric functions. However, we can illustrate the importance of dynamical correlations by varying the mass ratio in our MD simulations. The importance of these correlations is expected to increase as the mass ratio approaches unity.

We run simulations for binary mixtures with several mass ratios. We keep the heavy species fixed as Yb and vary the mass of the light species. The densities of each species are $n_{\rm light} = 4.3 \times 10^9$ cm^{-3} and $n_{\rm heavy} = 1.3 \times 10^{10}$ cm^{-3}. The mass ratios of each mixture are indicated in Table I.

TABLE I. Mass ratios and their square roots of the different binary mixtures MD simulations. m_2 is the mass of the light species, while $m_1 = m_{\rm Yb}$ always. The name of the light species is representative of ions with similar mass ratio.

Mixture	m_2/m_1	$\sqrt{m_2/m_1}$	Mixture	m_2/m_1	$\sqrt{m_2/m_1}$
Yb–H	0.006	0.076	Yb–Ca	0.230	0.479
Yb–Be	0.052	0.228	Yb–Sr	0.504	0.710
Yb–Mg	0.144	0.379	Yb–Nd	0.828	0.910

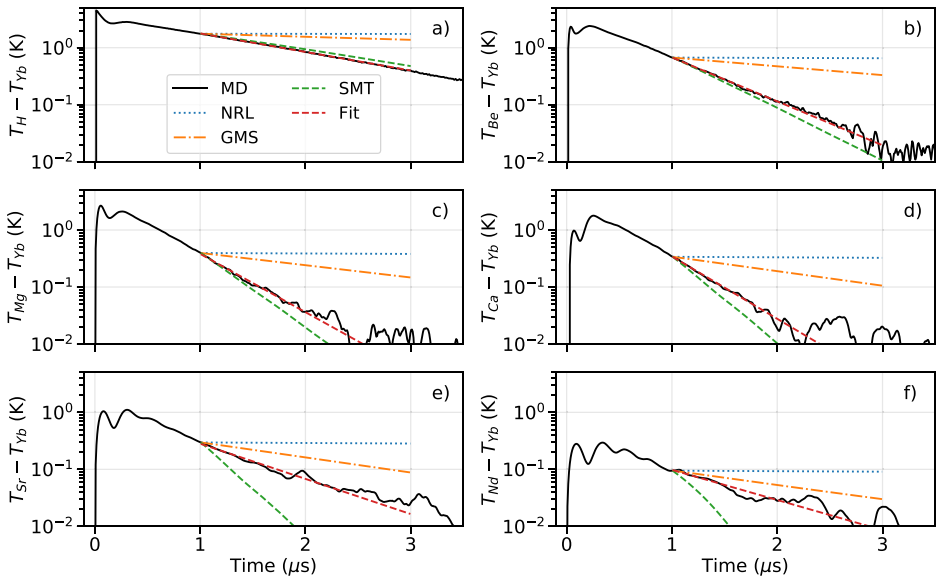

FIG. 3. Plots of the MD temperature difference $T_{\text{light}} - T_{\text{heavy}}$ for the six binary mixtures with different mass ratios compared with the prediction of the models described in Sec. II. (a) Yb–H mixture, (b) Yb–Be mixture, (c) Yb–Mg mixture, (d) Yb–Ca mixture, (e) Yb–Sr mixture, and (f) Yb–Nd mixture.

In Fig. 3, we compare the temperature difference with the three kinetic models for each mixture. The Hermite analysis described in Ref. 11 has been applied to each binary mixture in order to identify the time at which each species velocity distribution has relaxed to a Maxwellian. We find this time to be $\sim 1\ \mu$ s. This will be the starting time for the application of the static models.

In all cases, the NRL and GMS models from Sec. II drastically underestimate the relaxation rates. The SMT model shows better agreement at small mass ratios. Furthermore, the height of the highest peak of the temperature difference decreases with increasing mass ratio. The temperature difference in the Yb–Nd mixture is almost an order of magnitude smaller than the other mixtures and kinetic oscillations have not disappeared [see Fig. 3(f)]. This happens because the mass ratio, $m_{\text{Nd}}/m_{\text{Yb}} \sim 0.828$, is close to unity. Recall from Eq. (3) that the intra-species and inter-species relaxation times are proportional to the mass ratio. In this case, $(\propto \sqrt{m_{\text{Nd}}/m_{\text{Yb}}} = 0.910 \sim m_{\text{Nd}}/m_{\text{Yb}} = 0.828)$, indicating that correlational and kinetic processes happen simultaneously.

From Eq. (7), it is apparent that the dynamical correlations are included in the $\mathcal{S}$ term. Therefore, in order to further display the effect of dynamical correlations, we calculate the $\mathcal{S}$ using exponential fits to MD data and compare it to SMT predictions.

In Fig. 4, we plot the fitted and calculated $\mathcal{S}$ as a function of mass ratio. As the mass ratio decreases, the two methods converge. This underscores the importance of coupled modes in transport phenomena in plasma mixtures in which the ion mass ratio is near unity. Corrections of 20% are required even for a mass ratio of 0.1 at this density ratio.

We emphasize that this is not a complete analysis of the importance of coupled modes. This study has been performed for only one density ratio. Preliminary calculations indicate that results in Fig. 3 depend on the density ratio. In mixtures with a high concentration of the light species, the collective mode spectrum appears to be dominated by one single acoustic mode with a sound speed much faster than what is predicted by the QLCA.[28]

VII. CONCLUSION

We present an analysis of ion temperature relaxation in a strongly coupled binary plasma mixture. We derive a general temperature relaxation equation for binary mixtures that includes dynamical correlations. We demonstrate the shortcomings of the three popular kinetic models which include only static correlations. By comparing MD simulations with SMT predictions, the importance of dynamical correlations in collisional processes becomes apparent. These correlations become increasingly significant as the mass ratio approaches unity.

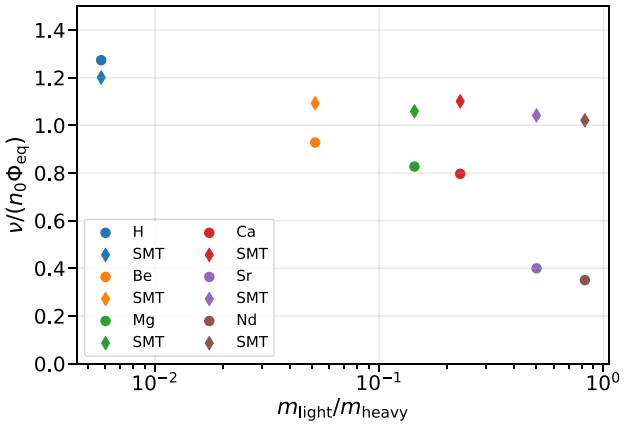

FIG. 4. Plot comparing the value of the collisional term $\mathcal{S}$ from Eq. (6) extracted from exponential fits to MD data (dots) and calculated from SMT.

Future work could explore different techniques for the identification of a hydrodynamic regime. The effect of plasma stoichiometry on dynamical correlations is an important and unexplored topic. Full dynamical calculations, with theories such as QLCA, for example, could provide helpful information regarding coupled-mode corrections to transport properties in plasma mixtures.

AUTHORS' CONTRIBUTIONS

R.T.S. and S.D.B. conceived and built the experiment, designed and carried out the laboratory measurements, and performed the experimental data reduction. L.G.S. and M.S.M. designed and performed the computer simulations and theoretical analysis and calculations. All authors contributed equally to the writing of the manuscript. All authors commented on the manuscript and agreed on its contents.

ACKNOWLEDGMENTS

We thank Dr. Jeffrey Haack of Los Alamos National Laboratory for useful conversations. M.S.M. and L.G.S. were supported by the U.S. Air Force Office of Scientific Research Grant No. FA9550–17-1–0394. R.T.S. and S.D.B. acknowledge support from the U.S. Air Force Office of Scientific Research Grant No. FA9550–17-1–0302 and the National Science Foundation Grant No. PHY-2009999.

The authors declare that they have no competing interest.

DATA AVAILABILITY

All data needed to evaluate the conclusions in the paper are present in the paper. The data that support the findings of this study are available from the corresponding author upon reasonable request.

REFERENCES

[1]T. Ma, P. K. Patel, N. Izumi, P. T. Springer, M. H. Key, L. J. Atherton, L. R. Benedetti, D. K. Bradley, D. A. Callahan, P. M. Celliers, C. J. Cerjan, D. S. Clark, E. L. Dewald, S. N. Dixit, T. Döppner, D. H. Edgell, R. Epstein, S. Glenn, G. Grim, S. W. Haan, B. A. Hammel, D. Hicks, W. W. Hsing, O. S. Jones, S. F. Khan, J. D. Kilkenny, J. L. Kline, G. A. Kyrala, O. L. Landen, S. L. Pape, B. J. MacGowan, A. J. Mackinnon, A. G. MacPhee, N. B. Meezan, J. D. Moody, A. Pak, T. Parham, H.-S. Park, J. E. Ralph, S. P. Regan, B. A. Remington, H. F. Robey, J. S. Ross, B. K. Spears, V. Smalyuk, L. J. Suter, R. Tommasini, R. P. Town, S. V. Weber, J. D. Lindl, M. J. Edwards, S. H. Glenzer, and E. I. Moses, "Onset of hydrodynamic mix in high-velocity, highly compressed inertial confinement fusion implosions," Phys. Rev. Lett. **111**, 085004 (2013).

[2]H. G. Rinderknecht, P. A. Amendt, S. C. Wilks, and G. Collins, "Kinetic physics in ICF: Present understanding and future directions," Plasma Phys. Controlled Fusion **60**, 064001 (2018).

[3]B. M. Haines, R. C. Shah, J. M. Smidt, B. J. Albright, T. Cardenas, M. R. Douglas, C. Forrest, V. Y. Glebov, M. A. Gunderson, C. E. Hamilton, K. C. Henderson, Y. Kim, M. N. Lee, T. J. Murphy, J. A. Oertel, R. E. Olson, B. M. Patterson, R. B. Randolph, and D. W. Schmidt, "Observation of persistent species temperature separation in inertial confinement fusion mixtures," Nat. Commun. **11**, 1 (2020).

[4]L. G. Stanton and M. S. Murillo, "Ionic transport in high-energy-density matter," Phys. Rev. E **93**, 043203 (2016).

[5]E. Vold, R. Rauenzahn, and A. N. Simakov, "Multi-species plasma transport in 1D direct-drive ICF simulations," Phys. Plasmas **26**, 032706 (2019).

[6]D. Rosenberger, N. Lubbers, and T. C. Germann, "Evaluating diffusion and the thermodynamic factor for binary ionic mixtures," Phys. Plasmas **27**, 102705 (2020).

[7]J. Clérouin, P. Arnault, B.-J. Gréa, S. Guisset, M. Vandenboomgaerde, A. J. White, L. A. Collins, J. D. Kress, and C. Ticknor, "Static and dynamic properties of multi-ionic plasma mixtures," Phys. Rev. E **101**, 033207 (2020).

[8]P. Grabowski, S. Hansen, M. Murillo, L. Stanton, F. Graziani, A. Zylstra, S. Baalrud, P. Arnault, A. Baczewski, L. Benedict, C. Blancard, O. Čertík, J. Clérouin, L. Collins, S. Copeland, A. Correa, J. Dai, J. Daligault, M. Desjarlais, M. Dharma-wardana, G. Faussurier, J. Haack, T. Haxhimali, A. Hayes-Sterbenz, Y. Hou, S. Hu, D. Jensen, G. Jungman, G. Kagan, D. Kang, J. Kress, Q. Ma, M. Marciante, E. Meyer, R. Rudd, D. Saumon, L. Shulenburger, R. Singleton, T. Sjostrom, L. Stanek, C. Starrett, C. Ticknor, S. Valaitis, J. Venzke, and A. White, "Review of the first charged-particle transport coefficient comparison workshop," High Energy Density Phys. **37**, 100905 (2020).

[9]T. Sprenkle, A. Dodson, Q. McKnight, R. Spencer, S. Bergeson, A. Diaw, and M. S. Murillo, "Ion friction at small values of the Coulomb logarithm," Phys. Rev. E **99**, 053206 (2019).

[10]S. D. Bergeson, S. D. Baalrud, C. L. Ellison, E. Grant, F. R. Graziani, T. C. Killian, M. S. Murillo, J. L. Roberts, and L. G. Stanton, "Exploring the crossover between high-energy-density plasma and ultracold neutral plasma physics," Phys. Plasmas **26**, 100501 (2019).

[11]R. Sprenkle, L. Silvestri, M. Murillo, and S. Bergeson, "Temperature relaxation in strongly-coupled binary ionic mixtures," Nature Portfolio (submitted) (2021).

[12]S. Ichimaru, *Statistical Plasma Physics* (CRC Press, Boca Raton, FL, 2004).

[13]J. R. Haack, C. D. Hauck, and M. S. Murillo, "A conservative, entropic multispecies BGK model," J. Stat. Phys. **168**, 826–856 (2017).

[14]A. S. Richardson, *2019 NRL Plasma Formulary* (US Naval Research Laboratory, 2019).

[15]D. Gericke, M. Murillo, and M. Schlanges, "Dense plasma temperature equilibration in the binary collision approximation," Phys. Rev. E **65**, 036418 (2002).

[16]M. W. C. Dharma-wardana and F. M. C. Perrot, "Energy relaxation and the quasiequation of state of a dense two-temperature nonequilibrium plasma," Phys. Rev. E **58**, 3705–3718 (1998).

[17]M. W. C. Dharma-wardana and F. M. C. Perrot, "Erratum: Energy relaxation and the quasiequation of state of a dense two-temperature nonequilibrium plasma [Phys. Rev. E **58**, 3705 (1998)]," Phys. Rev. E **63**, 069901 (2001).

[18]D. A. Chapman, J. Vorberger, and D. O. Gericke, "Reduced coupled-mode approach to electron-ion energy relaxation," Phys. Rev. E **88**, 013102 (2013).

[19]P. Mabey, S. Richardson, T. G. White, L. B. Fletcher, S. H. Glenzer, N. J. Hartley, J. Vorberger, D. O. Gericke, and G. Gregori, "A strong diffusive ion mode in dense ionized matter predicted by Langevin dynamics," Nat. Commun. **8**, 1 (2017).

[20]L. X. Benedict, J. N. Glosli, D. F. Richards, F. H. Streitz, S. P. Hau-Riege, R. A. London, F. R. Graziani, M. S. Murillo, and J. F. Benage, "Molecular dynamics simulations of electron-ion temperature equilibration in an SF_6 plasma," Phys. Rev. Lett. **102**, 205004 (2009).

[21]J. Daligault and G. Dimonte, "Correlation effects on the temperature-relaxation rates in dense plasmas," Phys. Rev. E **79**, 056403 (2009).

[22]L. X. Benedict, M. P. Surh, J. I. Castor, S. A. Khairallah, H. D. Whitley, D. F. Richards, J. N. Glosli, M. S. Murillo, C. R. Scullard, P. E. Grabowski *et al.*, "Molecular dynamics simulations and generalized Lenard-Balescu calculations of electron-ion temperature equilibration in plasmas," Phys. Rev. E **86**, 046406 (2012).

[23]G. Dimonte and J. Daligault, "Molecular-dynamics simulations of electron-ion temperature relaxation in a classical Coulomb plasma," Phys. Rev. Lett. **101**, 135001 (2008).

[24]L. G. Stanton and M. S. Murillo, "Unified description of linear screening in dense plasmas," Phys. Rev. E **91**, 033104 (2015).

[25]G. Hazak, Z. Zinamon, Y. Rosenfeld, and M. W. C. Dharma-wardana, "Temperature relaxation in two-temperature states of dense electron-ion systems," Phys. Rev. E **64**, 066411 (2001).

[26]G. J. Kalman and K. I. Golden, "Response function and plasmon dispersion for strongly coupled Coulomb liquids," Phys. Rev. A **41**, 5516–5527 (1990); "Quasilocalized charge approximation in strongly coupled plasma physics," Phys. Plasmas **7**, 14–32 (2000); "Erratum: 'Quasilocalized charge approximation in strongly coupled plasma physics' [Phys. Plasmas **7**, 14 (2000)]," **8**, 5064 (2001).

[27]L. Silvestri, G. J. Kalman, Z. Donkó, P. Hartmann, and H. Kählert, "Fano-like anti-resonances in strongly coupled binary Coulomb systems," Europhys. Lett. **109**, 15003 (2015).

[28]L. G. Silvestri, "The dynamical structure functions of strongly coupled binary charged systems," Ph.D. thesis (Boston College, Graduate School of Arts and Sciences, 2019).
[29]G. J. Kalman, P. Hartmann, Z. Donkó, K. I. Golden, and S. Kyrkos, "Collective modes in two-dimensional binary Yukawa systems," Phys. Rev. E **87**, 043103 (2013).
[30]G. J. Kalman, Z. Donkó, P. Hartmann, and K. I. Golden, "Strong coupling effects in binary Yukawa systems," Phys. Rev. Lett. **107**, 175003 (2011).
[31]G. Kalman, Z. Donkó, P. Hartmann, and K. I. Golden, "Second plasmon and collective modes in binary Coulomb systems," Europhys. Lett. **107**, 35001 (2014).
[32]Y. C. Chen, C. E. Simien, S. Laha, P. Gupta, Y. N. Martinez, P. G. Mickelson, S. B. Nagel, and T. C. Killian, "Electron screening and kinetic-energy oscillations in a strongly coupled plasma," Phys. Rev. Lett. **93**, 265003 (2004).
[33]M. S. Murillo, "Ultrafast dynamics of strongly coupled plasmas," Phys. Rev. Lett. **96**, 165001 (2006).
[34]See https://murillo-group.github.io/sarkas/ for Sarkas' documentation (last accessed October 2020).
[35]G. Dharuman, L. G. Stanton, J. N. Glosli, and M. S. Murillo, "A generalized Ewald decomposition for screened Coulomb interactions," J. Chem. Phys. **146**, 024112 (2017).